BIOCHEMISTRY
including biophysical chemistry & molecular biology

Article

pubs.acs.org/biochemistry

Spectroscopic Studies of Single and Double Variants of M Ferritin: Lack of Conversion of a Biferrous Substrate Site into a Cofactor Site for O_2 Activation

Yeonju Kwak,[†] Jennifer K. Schwartz,[†] Suranjana Haldar,[‡] Rabindra K. Behera,[‡] Takehiko Tosha,[‡] Elizabeth C. Theil,*[,‡,§] and Edward I. Solomon*[,†]

[†]Department of Chemistry, Stanford University, Stanford, California 94305, United States

[‡]Council for BioIron at CHORI (Children's Hospital Oakland Research Institute), Oakland, California 94609, United States

[§]Department of Molecular and Structural Biochemistry, North Carolina State University, Raleigh, North Carolina 27695-7622, United States

Supporting Information

ABSTRACT: Ferritin has a binuclear non-heme iron active site that functions to oxidize iron as a substrate for formation of an iron mineral core. Other enzymes of this class have tightly bound diiron cofactor sites that activate O_2 to react with substrate. Ferritin has an active site ligand set with 1-His/4-carboxylate/1-Gln rather than the 2-His/4-carboxylate set of the cofactor site. This ligand variation has been thought to make a major contribution to this biferrous substrate rather than cofactor site reactivity. However, the Q137E/D140H double variant of M ferritin, has a ligand set that is equivalent to most of the diiron cofactor sites, yet did not rapidly react with O_2 or generate the peroxy intermediate observed in the cofactor sites. Therefore, in this study, a combined spectroscopic methodology of circular dichroism (CD)/magnetic CD (MCD)/variable temperature, variable field (VTVH) MCD has been applied to evaluate the factors required for the rapid O_2 activation observed in cofactor sites. This methodology defines the coordination environment of each iron and the bridging ligation of the biferrous active sites in the double and corresponding single variants of frog M ferritin. Based on spectral changes, the D140H single variant has the new His ligand binding, and the Q137E variant has the new carboxylate forming a μ-1,3 bridge. The spectra for the Q137E/D140H double variant, which has the cofactor ligand set, however, reflects a site that is more coordinately saturated than the cofactor sites in other enzymes including ribonucleotide reductase, indicating the presence of additional water ligation. Correlation of this double variant and the cofactor sites to their O_2 reactivities indicates that electrostatic and steric changes in the active site and, in particular, the hydrophobic nature of a cofactor site associated with its second sphere protein environment, make important contributions to the activation of O_2 by the binuclear non-heme iron enzymes.

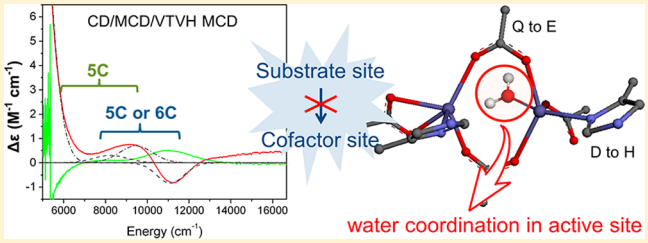

Binuclear non-heme iron enzymes are an expanding class that carries out a variety of important reactions through dioxygen activation. Some of the most-studied enzymes in this class are ribonucleotide reductase (RNR),[1] which initiates radical chemistry to generate DNA building blocks, methane monooxygnease (MMO),[2] which hydroxylates methane to methanol, and Δ^9 desaturase (Δ^9D),[3] which inserts a double bond into fatty acids to produce lipid precursors. Crystallographic[4−6] and spectroscopic[7−10] studies have shown that these enzymes share a common 2-His/4-carboxylate ligand set where the diiron core in the biferrous active site is weakly magnetically coupled through two μ-1,3-carboxylate bridges. In these enzymes, the diiron site serves as a "cofactor", since it rapidly reacts with and activates O_2 and remains tightly bound throughout the reaction with substrate. Diferric-peroxo (DFP) intermediates have been observed[11−13] for all three of the above enzymes, which further convert into high-valent intermediates in RNR[14] and MMO.[15]

In contrast, the two ferrous ions are the "substrate" in the ferritins, as these enzymes perform a ferroxidase reaction to generate an oxo/hydroxo diferric product, which is then released from the site and stored in a nanocage as a ferric mineral core.[16] Each catalytic subunit contains a ferroxidase site that catalyzes this reaction between the biferrous center and O_2. A similar DFP intermediate from fast dioxygen reaction has been observed during the ferroxidation reaction.[17,18]

To understand the unique ferroxidase reaction in the substrate site of the ferritins, crystallographic and spectroscopic studies on bullfrog M ferritin have been performed.[17−30] Crystal structures of the active sites are shown in Figure 1. These crystal structures were obtained with divalent proxies (i.e., Mg(II), Co(II), and Cu(II)) for Fe(II), since the Fe(II)

Received: October 4, 2013
Revised: December 17, 2013
Published: January 7, 2014

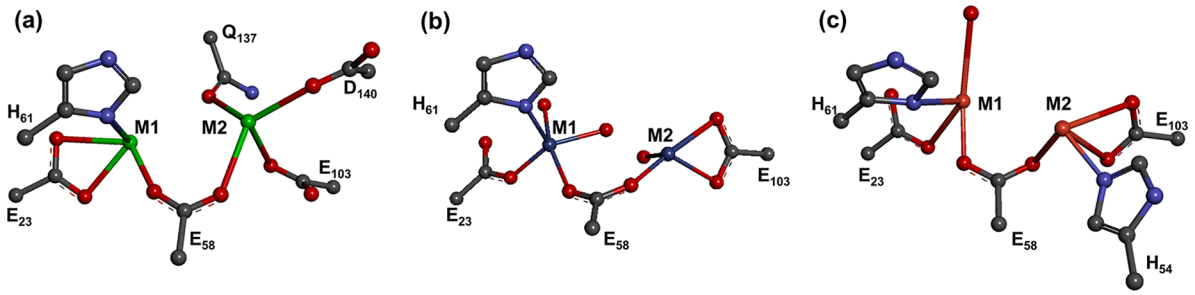

Figure 1. Proposed WT ferritin biferrous active site from crystal structure with (a) Mg^{2+} (RCSB 1MFR, ref 20); (b) Co^{2+} (RCSB 3KA4, ref 27); and (c) Cu^{2+} (RCSB 3RE7, ref 30).

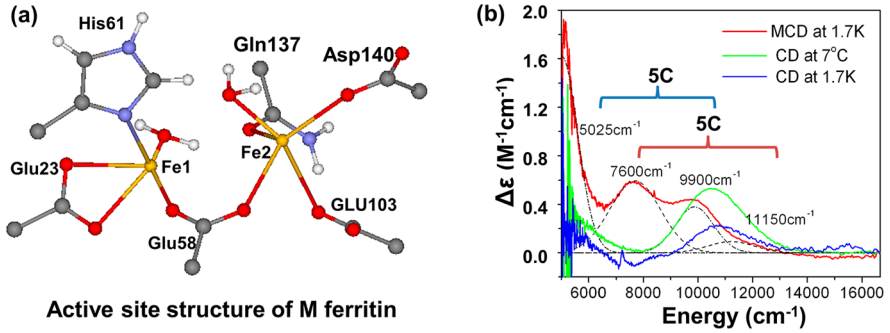

Figure 2. (a) Proposed active site structure of WT M ferritin; and (b) its CD and MCD spectra. Coordination number for each iron site was obtained from VTVH MCD data. Adapted and modified from ref 24.

substrate rapidly reacts with O_2, and thus only ferric structures have been observed in the vicinity of the ferritin active sites after soaking ferritin protein crystals in solutions of Fe(II).[30,31] For this reason, protein crystallography of ferritin is a less informative probe of metal binding at the active site than for the related proteins where diiron sites remain occupied. Although the three crystal structures with different divalent metals display variations in the ligand set of one metal site (M2 in Figure 1) and the binding mode of the terminal carboxylate to the other metal site (M1, Figure 1),[20,27,30] it is clear that the substrate site has a coordinating environment that is distinct from that of the cofactor sites, as it has only one μ-1,3 carboxylate bridge and is more weakly bound to the protein (Figure 1). This structural difference allows the diferric product to leave the active site for formation of the ferric mineral core.

A combined spectroscopic methodology of circular dichroism (CD), magnetic CD (MCD), and variable-temperature, variable-field (VTVH) MCD has been applied to define the wild-type (WT) substrate site in M ferritin under biologically relevant solution conditions,[24] enabling its comparison to the binuclear non-heme iron cofactor sites.[8−10,24] CD and MCD spectroscopies probe the ligand-field (LF) transitions characteristic of the coordination of each iron in the active site. These transitions can be correlated to a specific iron center based on their VTVH MCD behavior.[32] This methodology also determines the zero-field splitting (ZFS, D (axial), E (rhombic)) of each Fe(II) and exchange coupling (J) between two iron centers (reflecting bridging).

The spectra obtained for the biferrous active site of the ferritin showed 4 LF transitions that were paired by their VTVH MCD behaviors. Based on their LF splitting patterns, the two sets of transitions identified two inequivalent 5-coordinate irons in the active site (Figure 2b). This result indicates that the substrate site is ligated by one water on each iron in addition to the protein-based ligands, as shown in Figure 2a, with an open coordinate position on each iron that could react with O_2 in a bridged structure. The water in the active site was thought to be important in the formation of the diferric oxo/hydroxo species, since the protons provided by the coordinated water would facilitate the decay of the DFP intermediate.

In a study by Tosha et al., the substrate site in M ferritin was modified by substituting two of the natural amino acids of the Fe2 site with those found in the cofactor sites, creating the Q137E/D140H double variant.[25] However, the kinetic results indicate that despite having the same ligand set, the double variant was not converted into a cofactor site in that the double variant exhibited very slow O_2 reaction without the observed formation of a DFP intermediate.

In the present study, we have applied CD/MCD/VTVH MCD spectroscopic methodology to define the geometric and electronic structure of the biferrous active site in the Q137E/D140H double variant of M ferritin and to correlate this structure with its slow O_2 reactivity. The CD/MCD/VTVH MCD spectra of two single variants (D140H and Q137E) were obtained in parallel and compared to the WT M ferritin spectra (Figure 2b) to evaluate the structural contribution associated with each ligand substitution, in order to elucidate the double-variant active site ligation. Comparison of the ferritin double variant active site obtained in this study to that of D84E RNR, which has the same ligand set but rapidly reacts with O_2, revealed important factors required for an effective O_2 reaction.

EXPERIMENTAL SECTION

1. Sample Preparation. MOPS buffer (Sigma-Aldrich), sodium chloride (EMD Chemicals, Inc.), deuterium oxide (99.9 atom % D, Cambridge Isotope Laboratories), d_3-glycerol (98 atom % D, Cambridge Isotope Laboratories), and ferrous sulfate heptahydrate (Baker) were purchased commercially and

dx.doi.org/10.1021/bi4013726 | Biochemistry 2014, 53, 473−482

used as obtained. Before being cycled into the glovebox (<1 ppm O_2), D_2O was made anaerobic by pumping it with argon gas (99.9% pure) for ∼5 h, and d_3-glycerol was degassed by heating it for ∼8 h under vacuum (10^{-3} Torr). Fe(II) stock solutions, used for reconstitution of the apoprotein, were freshly prepared before each experiment by adding anaerobic D_2O to a premeasured amount of solid ferrous sulfate in the glovebox.

A QuikChange Mutagenesis kit (Stratagene) was used for site-directed mutagenesis on frog M-ferritin in pET-3a, and recombinant ferritin variants were expressed in *Escherichia coli*, and then purified as previously described.[22,25] To remove iron from the core and potential binding sites, anaerobic reductive dialysis was performed in the presence of dithiothreitol.[24] For near-infrared (NIR) MCD measurements, the protein buffer solution was exchanged with a deuterium oxide buffer solution of 100 mM MOPS buffer (with100 mM NaCl) at pD = 7.0 until D_2O comprised more than 99.5% of the solvent. This protein solution was concentrated to 1−7 mM diiron active centers (0.04−0.3 mM protein nanocages) and degassed by rapidly purging with vacuum and argon cycles for ∼30 min.

Samples were studied in the absence of dioxygen (glovebox with an N_2 atmosphere). CD samples were prepared by adding incremental amounts of Fe(II) stock solution to the degassed apoprotein solution and incubating for ∼15 min. An anaerobic quartz cuvette was used, and the sample temperature was kept constant by a circulating water bath. The biferrous active site was also monitored by CD for any effect on the active site due to the glycerol. MCD samples were prepared by adding 2 Fe(II)/active site (determined based on anaerobic CD titration results; see Supporting Information) and rapidly mixing the protein solution with d_3-glycerol (50% v/v for the final concentration) until the sample became homogeneous. The protein samples were then injected into the MCD cell (with a 0.2−0.3 cm^{-1} thick spacer between two quartz windows), and immediately frozen in liquid N_2.

2. Spectroscopic Methods. NIR (600−2000 nm; 5000−16 666 cm^{-1}) CD and MCD data were collected on a Jasco J730 spectrapolarimeter operating with a liquid N_2-cooled InSb detector. The MCD spectra were obtained at various fields up to 7 T and temperatures between 1.6 and 15 K, using an Oxford magnet (either SM 4−7T or SM 4000−7T). The sample temperature was measured with a calibrated Cernox resistor (Lakeshore Cryogenics) inserted into the MCD cell. For each field and temperature, MCD spectra were baseline-corrected by subtracting the apoprotein spectrum and by averaging the (+) and (−) signals. VTVH MCD data were collected for 7 isotherms (1.8 K, 3 K, 5 K, 7.5 K, 10 K, 15 K, 25 K) at variable fields (0 T, 0.7 T, 1.4 T, 2.1 T, 2.8 T, 3.5 T, 4.2 T, 4.9 T, 5.6 T, 6.3 T, 7.0 T), and normalized to the observed intensity at lowest temperature and highest field (1.8 K, 7 T) for all isotherms taken at a given wavelength.

The CD and MCD spectra were simultaneously fit with Gaussian bandshapes to find the minimum number of peaks required. The VTVH MCD data were fit using the approaches described in the Supporting Information. A goodness-of-fit parameter and visual comparison of the simulations to the data with error bars were used to determine final fit results.

RESULTS AND ANALYSIS

1. D140H Variant (Reported as EQH mutant in ref 25). The D140H single amino acid substitution changes the Asp140 in Figure 2a to a His residue. If this His binds to the Fe2 site, only one of the two Fe(II) centers should be affected by this ligand change. The CD and MCD spectra of this variant are shown in Figure 3a and are different from those of the biferrous

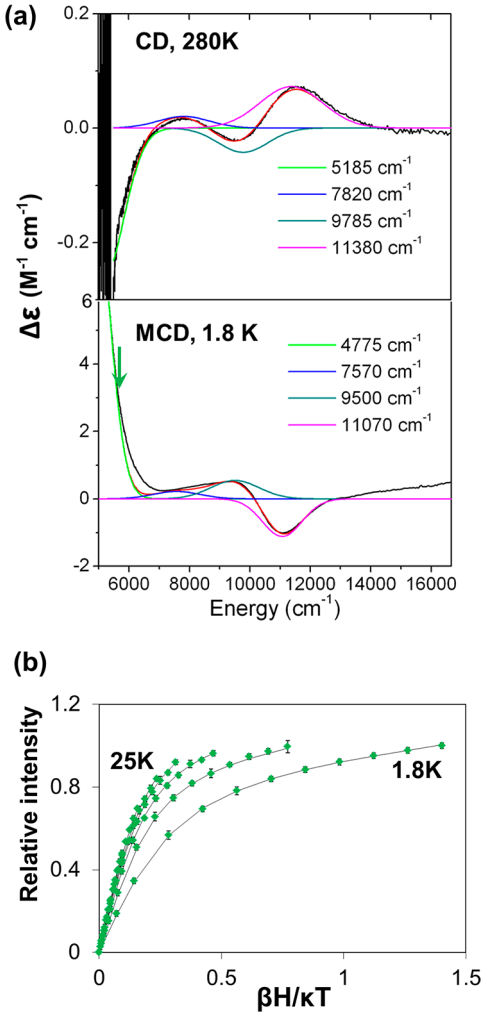

Figure 3. Spectra of the D140H ferritin single variant: (a) CD (280 K) spectra (top), and MCD (1.8 K, 7 T) spectra (bottom) of the biferrous active site in the D140H ferritin single variant. The experimental data are shown in the black line and the Gaussian bands from simultaneous peak fit are shown in color (overall fit, red; each peak, green, blue, cyan, and pink). Spectra require 4 LF transitions from two inequivalent irons. Arrow indicates the energy where VTVH data were collected; (b) VTVH data collected at 5530 cm^{-1} (green points with error bars) and the obtained doublet fit (solid line).

active site in WT ferritin in Figure 2b. The CD data show changes in more than two features in the spectrum, reflecting the sensitivity of CD to conformational changes in the vicinity of the site. MCD, by contrast, focuses directly on the electronic structure of the biferrous center. All the transitions in the D140H ferritin MCD spectrum are at energies similar to those of the WT site, indicating that this site has two inequivalent 5-coordinate (5C) iron centers. However, relative to the WT MCD spectrum in Figure 2b, this alteration perturbs the feature at 7600 cm^{-1}, which loses intensity, and the feature at 11 100 cm^{-1}, which changes sign from positive to negative (Figure 3a, bottom). This perturbation of two LF transitions indicates that the His ligand binds to one of the two ferrous centers of the

dx.doi.org/10.1021/bi4013726 | *Biochemistry* 2014, 53, 473−482

active site and that the two perturbed LF transitions are associated with that Fe. From Figure 2, the His would coordinate to Fe2.

The VTVH MCD data on the D140H ferritin were collected at 5530 cm^{-1} (arrow in Figure 3a) and fit using the two methods (equations S1−S3) in Supporting Information. Each ferrous center has a ground state with $S = 2$. These two iron centers can undergo both single center ZFS and exchange coupling between the centers, thus leading to a complicated set of ground state non-Kramer doublets for the biferrous active site (see SI pages S2 − S3). In the first method, sums of non-Kramers doublets are used to fit the ground state parameters (g-tensor with M_s value) and the excited state energies of the combined metal site (equation S1, doublet model). Because exchange coupling (J) between two ferrous centers is comparable to the ZFS of each iron (D, E), both J and ZFS (D, E) were considered together in a spin-Hamiltonian analysis of the doublet fit results to describe the ground state electronic structures (equation S2). In the second method, each electronic transition was correlated to a specific iron center using the fact that the MCD intensity is proportional to the spin-expectation values of the single iron center in the binuclear ferrous wavefuctions (equation S3, spin-projection model).

From the doublet fit, the lowest doublet gave the parameters of $g_{\|} = 8$ and $\delta_0 = 4.1$ cm^{-1}, which indicate an $M_s = \pm 2$ ground state. At around 15 K, a low-lying excited state starts to populate, requiring an additional excited-state doublet to fit the VTVH MCD data in Figure 3b. The best fit was obtained with $g_{\|} = 4$, which is associated with the $M_s = \pm 1$ sublevel, at an excited state energy of ~6 cm^{-1}.

A spin-Hamiltonian analysis was then used to define the range of J, D, and E/D values for the biferrous site associated with the doublet fit parameters obtained above. A fit of the VTVH MCD data in Figure 3b to the spin-Hamiltonian gives -15 $cm^{-1} < D_1 < -12$ cm^{-1} ($E_1/D_1 = 0.3$−0.33), 10 $cm^{-1} < D_2 < 12$ cm^{-1} ($E_2/D_2 = 0.2$−0.25) with -1 $cm^{-1} < J < 0$ cm^{-1}, showing that the two Fe(II) centers are weakly antiferromagnetically coupled and that the single mutation did not significantly perturb the weak bridging interaction present in the WT enzyme ($J \approx -0.3$ cm^{-1}).[33]

The saturation magnetization behavior of the data in Figure 3b was then correlated to a specific Fe(II) center, using the spin-projection model described in Supporting Information. From this analysis, the Fe(II) center associated with the transition at 4775 cm^{-1} in Figure 3a was shown to have a ZFS of -14.6 ± 1 cm^{-1} and $E/D \approx 0.33$ (Supporting Figure S4). This spin projection analysis also gives the exchange coupling $J \approx -0.16 \pm 0.15$ cm^{-1}, which is consistent with the spin-Hamiltonian analysis of the doublet model fit to the VTVH MCD data in Figure 3b.

2. Q137E Single Variant (reported as EED mutant in ref 25). The Q137E single amino acid substitution changes Gln137 (amide) in Figure 2a to a Glu residue (carboxylate), which is capable of binding to both iron sites (i.e., to form a second bridge). The CD and MCD spectra for this variant are shown in Figure 4a. Compared to the spectrum of WT ferritin (Figure 2b), the CD and MCD spectral features from both iron centers are perturbed. Their simultaneous Gaussian peak fit requires 3 LF transitions, at 4500, 8400, and 10 300 cm^{-1}. The band at 10 300 cm^{-1} could reflect an Fe site that is 5C (paired with the 4500 cm^{-1} transition) or 6C (paired with the 8400 cm^{-1} transition). However, the two bands at 10 300 cm^{-1} and 8400 cm^{-1} showed different binding behaviors in a CD titration

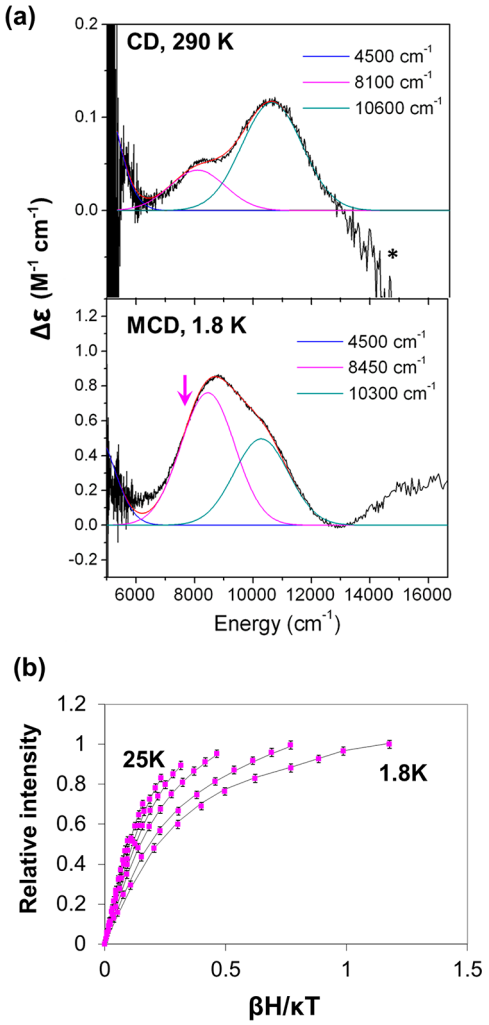

Figure 4. Spectra of the Q137E ferritin single variant: (a) CD (290 K) spectra (top) and MCD (1.8 K, 7 T) spectra (bottom) of the biferrous active site in the Q137E ferritin single variant. The experimental data are shown in the black line and the Gaussian bands from simultaneous peak fit are shown in color (overall fit, red; each peak, blue, pink, and cyan). Spectra require 3 LF transitions from two inequivalent iron centers. Arrow indicates the energy where VTVH data were collected. (b) VTVH data collected at 7570 cm^{-1} (pink points with error bars) and the obtained doublet fit (solid line) (* is the baseline due to the protein precipitation and is not affected by the magnetic field, indicating it is not a metal centered transition).

of the apoprotein with Fe(II) (Supporting Figure S5), indicating that these two transitions are from different iron centers. Based on the different binding behaviors, the band at 10 300 cm^{-1} (paired with 4500 cm^{-1}) reflects 5C iron site, and the band at 8400 cm^{-1} reflects another 5C iron site. Therefore, the biferrous active site coordination is determined to be 5C + 5C iron centers. Although the coordination numbers of both irons are the same as the WT ferritin, the large LF changes for both Fe(II) centers indicate that both irons are perturbed by the Q to E mutation, indicating formation of a second carboxylate bridge between the two Fe centers.

VTVH MCD data taken at 7570 cm^{-1} (arrow in Figure 4a) were analyzed using the methods (equations S1−S3) in Supporting Information. The doublet analysis gave ground-state parameters of $g_{\|} = 8$ and $\delta_0 = 3.0$ cm^{-1} ($M_s = \pm 2$) and an excited-state energy of ~6 cm^{-1}, with $g_{\|} = 4$ ($M_s = \pm 1$). The

dx.doi.org/10.1021/bi4013726 | Biochemistry 2014, 53, 473−482

spin-Hamiltonian analysis associated with these ground- and excited-state parameters gave the ZFS parameters, $-13\ cm^{-1} < D_1 < -10\ cm^{-1}$ ($E_1/D_1 = 0.3-0.33$), $9\ cm^{-1} < D_2 < 11\ cm^{-1}$ ($E_2/D_2 = 0.2-0.25$), and an exchange coupling $-1\ cm^{-1} < J < 0\ cm^{-1}$. It is noted that the J value is determined to be small and negative, which is similar to that of the WT enzyme and the D140H single variant. Based on proteins and model studies, μ-1,3 carboxylate bridges generally show small negative J's that are not necessarily additive (i.e., the number of μ-1,3 carboxylate bridges does not determine the magnitude of J). However, the data do show at least one μ-1,3 caboxylate bridge is present for all three active sites (WT and both single variants), because μ-1,1 carboxylate and μ-H_2O bridges both give small positive J values and an μ-OH bridge would have strong antiferro-coupling (i.e., $-J > 10\ cm^{-1}$).[34−36]

These VTVH MCD data were further correlated to a specific Fe(II) center, using the spin-projection model in equation S3, with the ZFS and J range obtained from the spin-Hamiltonian analysis. From this fitting, it was determined that the Fe(II) center associated with the 8400 cm^{-1} transition has a ZFS of $-11.7 \pm 0.8\ cm^{-1}$ and $E/D \approx 0.33$ (Supporting Figure S9). The exchange coupling was determined to be $J \approx -0.18 \pm 0.15\ cm^{-1}$, consistent with the results of fitting the doublet model.

3. Q137E/D140H Double Variant (reported as EEH mutant in ref 25). From the above results, the D to H mutation perturbed one Fe, indicating His binding to Fe2, and the Q to E mutation perturbed both irons, indicating bridge formation between two iron centers. Based on the above results, the double variant Q137E/D140H of ferritin should, in principal, correlate to the cofactor site of D84E RNR, which has the same ligand set. The CD, low-temperature (LT) CD, and MCD data for this double variant are shown in Figure 5. Compared to WT ferritin, the MCD spectrum of the double variant clearly shows the effect of His binding (MCD sign change for one iron site, Figure 2b vs Figure 5) and the LF transition energy slightly changed, which could be associated with the bridge formation. The simultaneous Gaussian fit for these spectra requires 4 LF transitions, at 4540, 8240, 9460, and 11 100 cm^{-1}. Thus, the two irons in the active site are inequivalent. The band at 4540 cm^{-1} reflects a 5C Fe site (paired with 9460 cm^{-1} or 11 000 cm^{-1}) or 4C (paired with 8240 cm^{-1}). Based on these possible pairings, the biferrous active site coordination in the double variant of ferritin is either 4C + 6C, or 5C + 5C (or 6C).

VTVH MCD data were collected for 3 LF transitions at the energies indicated by arrows in Figure 6a that minimize overlap with other bands. The data and their fits are shown in Figure 6b−d and analyzed using the methods described in Supporting Information (equations S1−S3). The doublet model gives ground-state parameters of $g_{||} = 8$ and $\delta_0 = 4.6\ cm^{-1}$ (i.e., an $M_s = \pm 2$ ground state) with an excited state at $\sim 7\ cm^{-1}$ with $g_{||} = 4$ (i.e., $M_s = \pm 1$). These parameters indicate that the two Fe(II) sites have different signs of D and are both quite rhombic. The spin-Hamiltonian analysis gives $-15\ cm^{-1} < D_1 < -13\ cm^{-1}$ ($E_1/D_1 = 0.3-0.33$), $12\ cm^{-1} < D_2 < 14\ cm^{-1}$ ($E_2/D_2 = 0.2-0.25$), and $-1\ cm^{-1} < J < 0\ cm^{-1}$. The J value indicates that the double variant also has weak antiferromagnetic coupling between the two Fe(II) centers. To pair the LF transitions and determine the coordination environment of each Fe(II), the spin-projection fitting of the VTVH MCD data was performed. Based on this analysis, the transitions at 4540 cm^{-1} and 9460 cm^{-1} are associated with the iron site with $D \approx -14.9 \pm 1.0\ cm^{-1}$ and $E/D \approx 0.33$ (Supporting Figures S12 and S13),

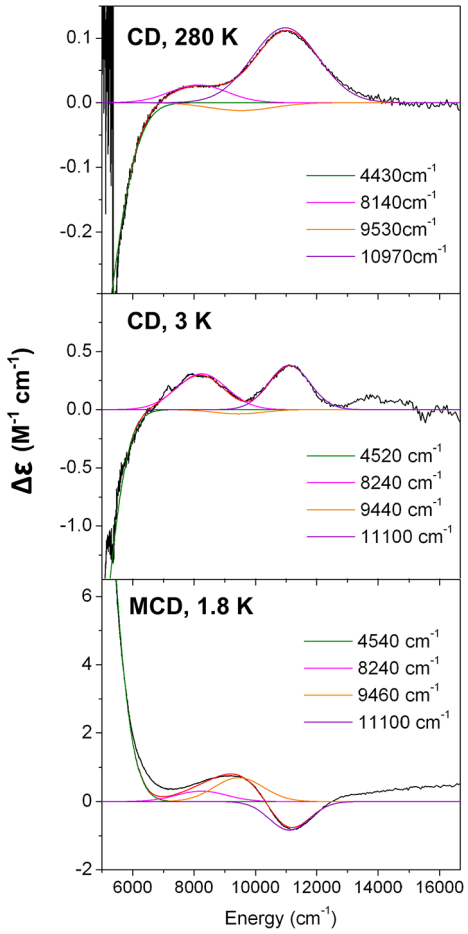

Figure 5. Spectra of the Q137E/D140H ferritin double variant: CD (280 K) spectra (top), low temperature CD (3K) spectra (middle), and MCD (1.8 K, 7T) spectra (bottom) of the biferrous active site in the Q137E/D140H ferritin double variant. The experimental data are shown in the black line and the Gaussian bands from simultaneous peak fit are shown in color (overall fit, red; each peak, green, pink, orange, and purple). Spectra require 4 LF transitions from two inequivalent irons.

and the transition at 11 100 cm^{-1} is associated with an iron site with $D \approx +13.6 \pm 0.8\ cm^{-1}$ and $E/D \approx 0.2$ (Supporting Figure S14). The exchange coupling is $J \approx -0.15 \pm 0.15\ cm^{-1}$. The Fe(II) with LF transitions at 4540 cm^{-1} and 9460 cm^{-1} is 5C, and the second Fe(II) with transitions at 8240 cm^{-1} and 11 000 cm^{-1} is either 5C or 6C, as the LF splitting for that iron site ($\sim$3000 cm^{-1}) is in a range that can be consistent with both. The ground and excited state parameters obtained for the single and double variants are summarized and compared to those of WT ferritin in Table 1.

DISCUSSION

The combination of CD, MCD, and VTVH MCD spectroscopies has been applied to the biferrous active site in the Q137E/D140H double variant of M ferritin that converts the ligand set of the ferroxidase site into one that is equivalent to the diiron cofactor site in D84E RNR. However, this double variant site has a different geometric and electronic structure compared to that of the cofactor site in D84E RNR that correlates with its much decreased O_2 reaction rate. The ferritin double variant has 4 LF transitions, which are paired as shown in Figure 7a, indicating that the two irons are 5C + 5C (or 6C),

dx.doi.org/10.1021/bi4013726 | Biochemistry 2014, 53, 473−482

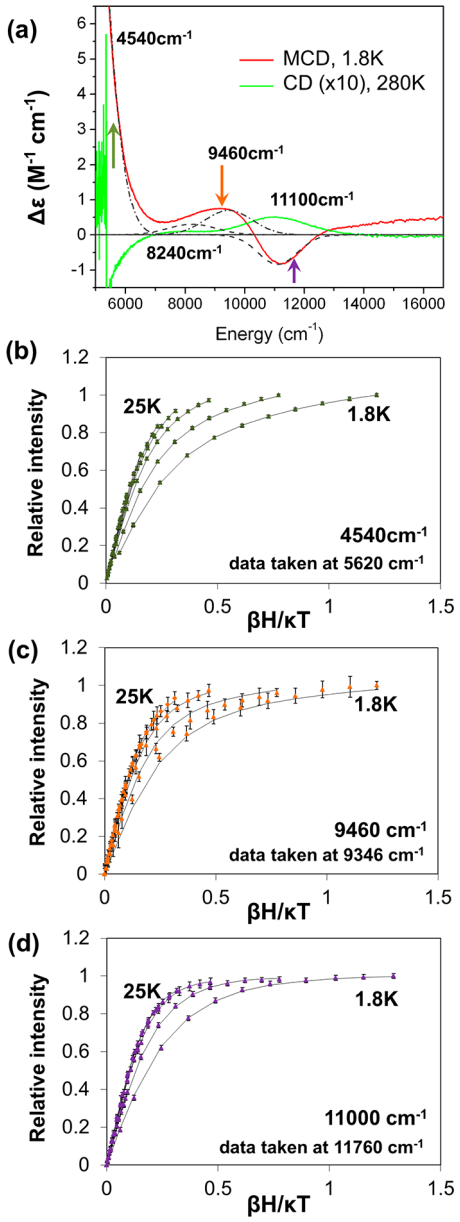

Figure 6. Spectra of the Q137E/D140H ferritin double variant: (a) Overlay of CD (280 K) and MCD (1.8 K) spectra. Gaussian-resolved peaks are shown as black dashed lines (– – – or – · – for the two different Fe(II) sites). Peaks at 4540 and 9460 cm^{-1} are assigned to Fe1 and peaks at 8240 and 11 100 cm^{-1} are assigned to Fe2, based on the three VTVH data sets, and their spin-projection fits shown in (b) – (d). Arrows indicate the energy where VTVH data were collected. Band at 8240 cm^{-1} is too small for VTVH data collection. VTVH data for each band (colored points with error bars) and spin-projection fit (solid line) are shown in (b), (c), and (d); (b) 4540 cm^{-1} band (data taken at 5620 cm^{-1}); (c) 9460 cm^{-1} band (data taken at 9346 cm^{-1}); and (d) 11 100 cm^{-1} band (data taken at 11 760 cm^{-1}).

while the biferrous site in D84E RNR has 3 LF transitions, which are paired as shown in Figure 7b, indicating 5C + 4C iron coordination.[8] Therefore, the coordination environment at the active sites of ferritin double variant is more saturated than that of D84E RNR. This requires the presence of at least one extra ligand in the double variant in ferritin either from the terminal carboxylate or from water. If the active site of the ferritin double variant did not have a water ligand, the 5C + 5C coordination would require that the two terminal carboxylates have bidentate binding at both iron centers. In this case, only two LF transitions from two similar ferrous centers would be observed, as found for the resting Δ^9D active site (Figure 7c).[10] However, the four LF transitions observed in the ferritin double variant indicate that the two ferrous ions in the active site possess inequivalent coordination environments. Therefore, with two bridging carboxylates, if one iron has a terminal bidentate carboxylate then the second would possess at least one water ligand.

Additional water coordination to one of the irons in the active site of the ferritin double variant would explain the difference in O_2 reactivities between this double variant site and a cofactor site as in D84E RNR. While it is possible to form the oxidized ferric species by iron auto-oxidation, the fact that the iron oxidation rate of this double variant (0.2 s^{-1}) is still an order of magnitude faster than auto-oxidation in the L subunit recombinant ferritin (~0.01 s^{-1}), which has no functional catalytic site,[22,25] indicates that the iron oxidation observed in the double variant reflects the reaction of O_2 with the biferrous active site, likely through a DFP intermediate. The rate constants for the O_2 reaction with the biferrous site (through a DFP, k_1) and the decay of the DFP (k_2) were estimated for the double variant (eq 1) and compared to those of D84E RNR (Table 2).

$$2\text{Fe(II)} + O_2 \xrightarrow{k_1} \text{Diferric-peroxo (DFP)} \xrightarrow{k_2} \text{Fe(III)–O(H)–Fe(III)} \quad (1)$$

Since a peroxo intermediate was not observed in the double variant, the DFP formation rate should be limiting, and the DFP rapidly decay (relative to k_1) to form the diferric–oxo(hydroxo) species. Therefore, k_1 is calculated from the kinetic data in ref 25 based on the initial diferric–oxo(hydroxo) formation rate (monitored $\Delta A_{350\ nm}$), and the lower limit of k_2 is estimated by assuming that the DFP intermediate would not be observed when $A_{650\ nm} < 0.01$. As shown in Table 2, the k_1 for the rate of the O_2 reaction of the double variant is 2 orders of magnitude slower than that of D84E RNR, while the lower limit of the k_2 value is similar between the double variant and D84E RNR. This decreased rate of DFP-formation could result from the presence of an active site water ligand in the double variant relative to D84E RNR, as it could block O_2 binding or alter the orientation of the redox active orbitals required for O_2 bridging. Therefore, although the protein-derived ligands are the same as those of a cofactor site, the presence of additional water ligation in the double variant active site of ferritin limits its ability to activate O_2. Interestingly, WT ferritin, which has a 5C + 5C active site, thus an additional ligand relative to the D84E RNR cofactor site, has comparable DFP formation and decay rates to D84E RNR (Table 2). These rates suggest that WT ferritin has the optimal orientation of the open coordination positions on both Fe(II) to allow O_2 to react in the bridging mode required for $2e^-$ reduction.[37] Based on the active site structure resulting from the spectroscopic studies in ref 24 (Figure 2a), the orientations of the open coordination positions in WT ferritin would derive from H-bonding of the coordinated water to the Q137 and D140 ligands. These water ligands would also contribute to the rapid DFP decay through proton donation to efficiently complete the ferroxidase reaction.

While the hydrophilic environment of the active site, which provides the additional water ligand in the double variant, is important in limiting the O_2 reaction rate, electrostatic and

dx.doi.org/10.1021/bi4013726 | Biochemistry 2014, 53, 473–482

Table 1. Comparison of Ground State Parameters, Spectral Features, Coordination Numbers of Each Iron, and the Exchange Coupling between Irons in the Active Site of WT M Ferritin, the D140H, the Q137E, and the Q137E/D140H Ferritin Variants

	WT ferritin[a]	D140H single variant	Q137E single variant	Q137E/D140H double variant
$g_{\parallel\,(GS)}$	8	8	8	8
δ_0	4.3	4.1	3.0	4.6
$g_{\parallel\,(ES)}$	4	4	4	4
ES energy (cm^{-1})	~3.4	~6	~6	~7
Fe1 Coord. Number/D (cm^{-1})	5C/−9.9	5C/−14.6	5C/−11.7	5C/−14.9
MCD Transitions (cm^{-1})	(5025, 9900)	(4775, 9500)	(4500, 10300)	(4540, 9460)
Fe2 Coord. Number/D (cm^{-1})	5C/+4.6	5C/+11.4	C/+10.5	5 or 6C/+13.6
MCD Transitions (cm^{-1})	(7600, 11500)	(7570, 11070)	(8400)	(8240, 11100)
Exchange coupling J (cm^{-1})	−0.3 ± 0.3	−0.16 ± 0.15	−0.18 ± 0.15	−0.15 ± 0.15

[a]Fit parameters are obtained from ref 33. Transitions for Fe1 and Fe2 are corrected based on the result from the single variant spectra in this work.

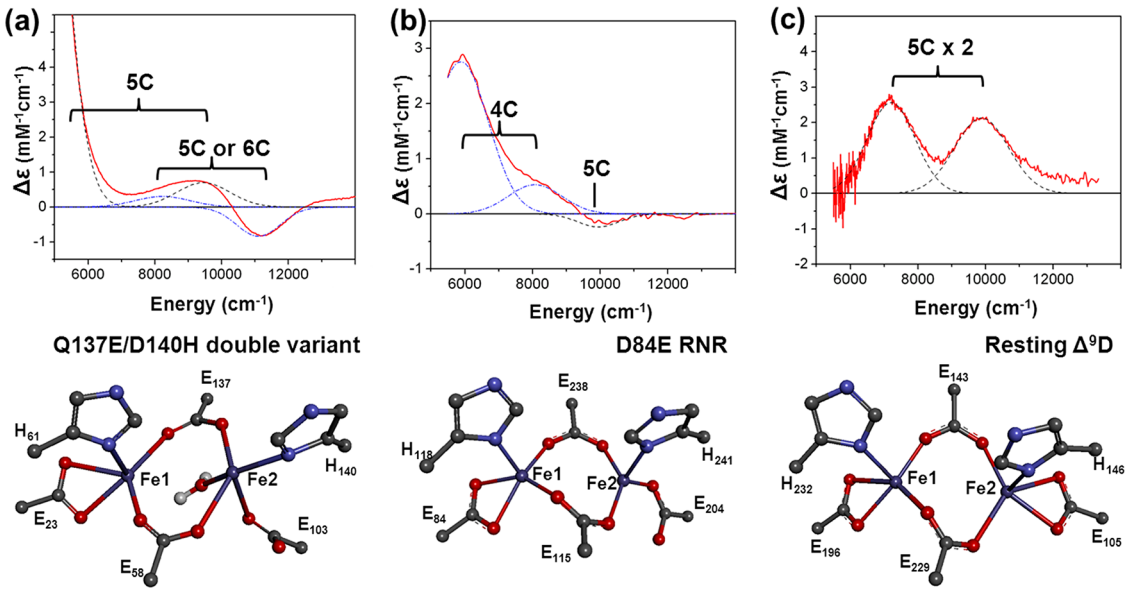

Figure 7. Comparison of MCD spectra and inferred active site structures of the Q137E/D140H ferritin double variant, D84E RNR, and resting Δ^9D: (a) MCD spectrum (top) and the active site structure (5C + 5C, bottom) of the Q137E/D140H ferritin double variant. Since Glu137 forms a second bridge, the water molecule on Fe1 (Figure 2) was replaced with the carboxylate oxygen ligand. Due to the His140 ligand replacing Asp140, the water molecule on Fe2 site is likely redirected relative to WT (Figure 2), which could affect the O_2 reactivity. There could be additional water binding or a change in the carboxylate binding mode (mono- vs bidentate E23 and E103); (b) D84E RNR, MCD spectrum (top) and matching crystal structure of the active site in D84E RNR (bottom), adapted and modified from refs 8 and 39; (c) Δ^9D, MCD spectrum (top) and matching crystal structure of the active site (bottom), adapted and modified from refs 6 and 10.

Table 2. Comparison of Initial O_2 Reaction Constants for Peroxo-Formation and Peroxo-Decay of the Q137E/D140H Ferritin Double Variant, D84E RNR, and WT M Ferritin

	k_1 (peroxo-formation, s^{-1})	k_2 (peroxo-decay, s^{-1})
Q137E/D140H variant[a,c]	0.20 ± 0.04	>2.2
D84E RNR[b]	58 ± 13	3.7 ± 0.7
WT M ferritin[a,c]	89 ± 2	7.4 ± 0.2

[a,c]Rate constant obtained (WT M ferritin) and calculated (Q137E/D140H variant) from ref 25 (20 °C); k_1 is calculated based on the initial diferric-oxo(hydroxo) formation rate (V_i monitored at $\Delta A_{350\ nm}$) based on the assumption that the DFP immediately decays to the diferric-oxo(hydroxo) species as soon as formed. The lower limit of k_2 is estimated by assuming that the DFP intermediate would not be observed when $A_{650\ nm} < 0.01$. [b]Rate constant obtained from ref 11, adjusted for subunit base for comparison with WT ferritin and the Q137E/D140H variant, 25 °C.

steric effect must also be considered. Mutation of the ligands could change the charge distribution (with no net charge change) around the active site, thus affect the dioxygen accessibility. In addition, steric effects, mostly caused by the mutation of the aliphatic chain into a ring (D to H), could reduce the O_2 reaction rate by blocking access to the active site, as suggested in the previous kinetic studies.[25] Because the dioxygen channel in ferritin is not well-defined, we focus on the active site pocket in WT ferritin and the double variant (WT ferritin obtained from crystal structure, RCSB 1MFR, ref 20; the double variant obtained by substituting the ligands from the WT crystal structure (Q137 to E and D140 to H), optimizing this structure with α-carbon position constraints using DFT,[38] and placing the optimized structure into the protein active site). The pocket volume of WT ferritin is calculated as ~70−100 $Å^3$ within 6 Å from the center of two irons. This volume is reduced to ~40−70 $Å^3$ in the double variant, which, however, is still large enough to bind both water and dioxygen (total ~30 $Å^3$). Therefore, the volume change in the active site pocket does not make a major contribution to the slower O_2 reaction rate of the double variant. Alternatively, this mutation does change in the shape of the active site pocket (Figure 8a vs b), which could

dx.doi.org/10.1021/bi4013726 | Biochemistry 2014, 53, 473−482

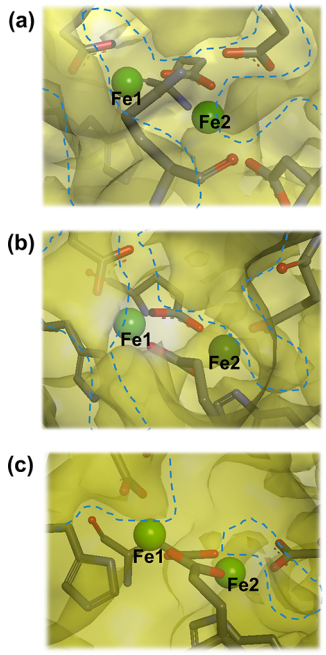

Figure 8. Active site pocket for small molecule access in (a) WT ferritin, RCSB 1MFR (ref 20); (b) Q137E/D140H double variant, optimized using DFT with the BP 86 functional with α-carbon constraints after amino acid substitution (Q137→E, D140→H); (c) D84E RNR, RCSB 1PIZ (ref 39). Active site pocket is indicated with darker colored spaces and blue dashed line. Mutation in the active site changes the shape of the active site pocket, which could limit the accessible orientation of dioxygen binding ((a) vs (b)). However, the double variant has 10−40 Å more space compared to the cofactor site in D84E RNR, which rapidly reacts with O_2 ((b) vs (c)).

reduce O_2 accessibility to the proper binding mode. However, D84E RNR (obtained from crystal structure, RCSB 1PIZ, ref 39) has an even smaller active site pocket (<30 Å^3) as shown in Figure 8c, yet shows a fast O_2 reaction rate (Table 2) compared to that of the double variant. This indicates that the dynamic properties of the protein can provide flexibility at the active site for O_2 binding. Therefore, although electrostatic and steric effects could contribute to the low k_1 in eq 1, the additional water ligand present in the double variant is likely the major contributor in limiting this O_2 reaction.

To obtain insight into the origin of the water ligation difference between the double variant of ferritin and D84E RNR, the overall protein scaffolds and their water accessibilities were compared (Figure 9). Even though both active sites share 4-helix bundle structures, D84E RNR has additional protein segments surrounding its 4-helix bundle, while the 4-helix bundles in the ferritin subunits are more exposed (Figure 9a). This difference in protein scaffolds would isolate the active site in D84E RNR from the solvent environment, relative to the active site in the double variant (Figure 9b). In addition, hydrophilic residues near the active site in ferritin could contribute to the water access through a channel observed in the crystal structure (Figure 10). (It was recently shown that that these hydrophilic residues are important for Fe(II) transfer from the ion channel to the active sites; R.K. Behera and E.C. Theil, in review).

Since ferritin has the task of rapidly collecting and storing free iron discharged from damaged iron proteins during oxidative stress,[40] the ability to detect and remove iron from the surroundings is an essential feature of its substrate site.

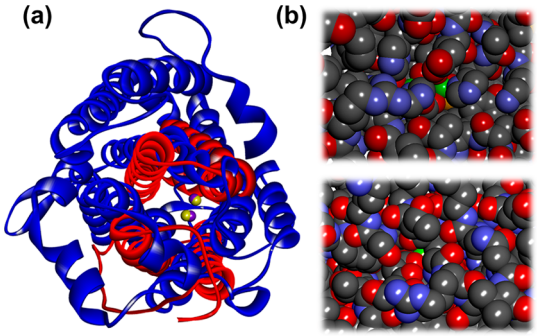

Figure 9. (a) Protein scaffold comparison between ferritin (red ribbon and yellow metal site) and D84E RNR (blue ribbon and violet metal site). D84E RNR has additional protein segments surrounding its 4-helix bundle, while the 4-helix bundles in the ferritin subunits are more exposed; (b) metal site (green) in ferritin Q137E/D140H variant from the view within the cage (top, changed Q to E and D to H from WT ferritin structure, RCSB 1MFR, ref 20) and metal site (green) in D84E RNR (bottom, obtained from crystal structure RCSB 1PIZ, ref 39).

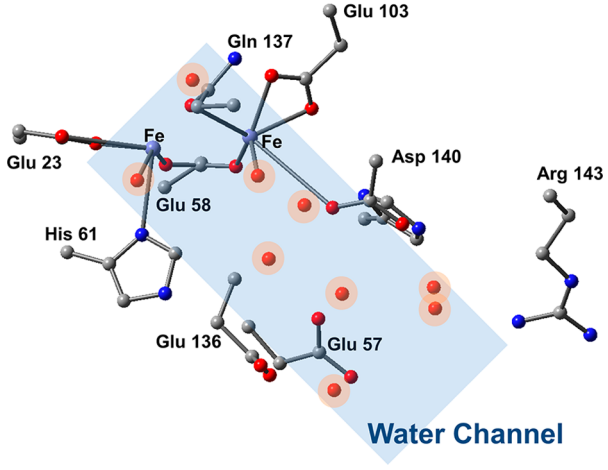

Figure 10. Diferric crystal structure of WT ferritin (RCSB 3RBC, ref 30) showing hydrophilic nature near the active site. This structure was chosen because it has a diiron active site, and this view was selected because ordered waters are in a direction allowing a view of the metal site in Figure 9b.

Therefore, ferritin active sites are optimized for iron substrate access, which is consistent with the hydrophilic protein environment near the biferrous site. Alternatively, the cofactor sites activate O_2 for reactions with substrate with a slower decay of the peroxo intermediate that allows its control for enzymatic function. The hydrophobic environment required in biferrous cofactor sites and the hydrophilic environment required in diiron substrate sites are achieved through first and second sphere contributions from the protein scaffold. Thus, the contributions of iron ligands to protein catalytic activity can be sufficiently modulated by the protein scaffold, to limit the ferritin double variant in its cofactor reactivity with the O_2.

■ ASSOCIATED CONTENT

Ⓢ Supporting Information

VTVH MCD data fit methods, binding affinity calculation methods, spectra from CD Fe(II) titration, spectra from MCD field dependence and temperature dependence, and VTVH MCD data fit with spin projection model. This material is available free of charge via the Internet at http://pubs.acs.org.

dx.doi.org/10.1021/bi4013726 | *Biochemistry* 2014, 53, 473−482

AUTHOR INFORMATION

Corresponding Authors

*Tel: 510-450-7670, E-mail: etheil@chori.org.
*Tel: 650-723-9104, E-mail: edward.solomon@stanford.edu.

Funding

This work was supported by an NSF Biochemistry Program Grant (MCB-0919027 to E.I.S.), an NIH Grant (DK-20251 to E.C.T.), a Japan Society for the Promotion of Science Postdoctoral Fellowship (to T.T.), and a Samsung scholarship (to Y.K.).

Notes

The authors declare no competing financial interest.

ACKNOWLEDGMENTS

We thank Dr. Xiaofeng Liu for the helpful discussion on the anaerobic reductive dialysis methods.

ABBREVIATIONS

CD, circular dichroism; MCD, magnetic circular dichroism; VTVH MCD, variable temperature, variable field magnetic circular dichroism; ZFS, zero field splitting (*D*: axial ZFS, *E*: rhombic ZFS); *J*, exchange coupling; RNR, ribonucleotide reductase; MMO, methane monooxygenase; Δ^9D, Δ^9 Desaturase; DFP, diferric-peroxo; WT, wild-type; LF, ligand field; NIR, near-infrared; LT, low temperature; ES, excited state; GS, ground state

REFERENCES

(1) Nordlund, P., and Reichard, P. (2006) Ribonucleotide reductases. *Annu. Rev. Biochem. 75*, 681−706.

(2) Tinberg, C. E., and Lippard, S. J. (2011) Dioxygen activation in soluble methane monooxygenase. *Acc. Chem. Res. 44*, 280−288.

(3) Fox, B. G., Lyle, K. S., and Rogge, C. E. (2004) Reactions of the diiron enzyme stearoyl-acyl carrier protein desaturase. *Acc. Chem. Res. 37*, 421−429.

(4) Logan, D. T., Su, X. D., Aberg, A., Regnström, K., Hajdu, J., Eklund, H., and Nordlund, P. (1996) Crystal structure of reduced protein R2 of ribonucleotide reductase: the structural basis for oxygen activation at a dinuclear iron site. *Structure 4*, 1053−1064.

(5) Whittington, D. A., and Lippard, S. J. (2001) Crystal structures of the soluble methane monooxygenase hydroxylase from *Methylococcus capsulatus* (bath) demonstrating geometrical variability at the dinuclear iron active site. *J. Am. Chem. Soc. 123*, 827−838.

(6) Lindqvist, Y., Huang, W., Schneider, G., and Shanklin, J. (1996) Crystal structure of Δ^9 stearoyl-acyl carrier protein desaturase from castor seed and its relationship to other di-iron proteins. *EMBO J. 15*, 4081.

(7) Yang, Y.-S., Baldwin, J., Ley, B. A., Bollinger, J. M., and Solomon, E. I. (2000) Spectroscopic and electronic structure description of the reduced binuclear non-heme iron active site in ribonucleotide reductase from *E. coli*: comparison to reduced Δ^9 desaturase and electronic structure contributions to differences in O_2 reactivity. *J. Am. Chem. Soc. 122*, 8495−8510.

(8) Wei, P.-P., Skulan, A. J., Mitić, N., Yang, Y.-S., Saleh, L., Bollinger, J. M., and Solomon, E. I. (2004) Electronic and spectroscopic studies of the non-heme reduced binuclear iron sites of two ribonucleotide reductase variants: comparison to reduced methane monooxygenase and contributions to O_2 reactivity. *J. Am. Chem. Soc. 126*, 3777−3788.

(9) Pulver, S., Froland, W. A., Fox, B. G., Lipscomb, J. D., and Solomon, E. I. (1993) Spectroscopic studies of the coupled binuclear non-heme iron active site in the fully reduced hydroxylase component of methane monooxygenase: comparison to deoxy and deoxy-azide hemerythrin. *J. Am. Chem. Soc. 115*, 12409−12422.

(10) Yang, Y.-S., Broadwater, J. A., Pulver, S. C., Fox, B. G., and Solomon, E. I. (1999) Circular dichroism and magnetic circular dichroism studies of the reduced binuclear non-heme iron site of stearoyl-ACP Δ^9-desaturase: substrate binding and comparison to ribonucleotide reductase. *J. Am. Chem. Soc. 121*, 2770−2783.

(11) Bollinger, J. M., Jr., Krebs, C., Vicol, A., Chen, S., Ley, B. A., Edmondson, D. E., and Huynh, B. H. (1998) Engineering the diiron site of *Escherichia coli* ribonucleotide reductase protein R2 to accumulate an intermediate similar to H_{peroxo}, the putative peroxodiiron (III) complex from the methane monooxygenase catalytic cycle. *J. Am. Chem. Soc. 120*, 1094−1095.

(12) Lee, S. K., Nesheim, J. C., and Lipscomb, J. D. (1993) Transient intermediates of the methane monooxygenase catalytic cycle. *J. Biol. Chem. 268*, 21569−21577.

(13) Broadwater, J. A., Ai, J., Loehr, T. M., Sanders-Loehr, J., and Fox, B. G. (1998) Peroxodiferric intermediate of stearoyl-acyl carrier protein Δ^9 desaturase: oxidase reactivity during single turnover and implications for the mechanism of desaturation. *Biochemistry 37*, 14664−14671.

(14) Sturgeon, B. E., Burdi, D., Chen, S., Huynh, B. H., Edmondson, D. E., Stubbe, J. A., and Hoffman, B. M. (1996) Reconsideration of X, the diiron intermediate formed during cofactor assembly in *E. coli* ribonucleotide reductase. *J. Am. Chem. Soc. 118*, 7551−7557.

(15) Shu, L., Nesheim, J. C., Kauffmann, K., Münck, E., Lipscomb, J. D., and Que, L. (1997) An $Fe^{IV}_2O_2$ diamond core structure for the key intermediate Q of methane monooxygenase. *Science 275*, 515−518.

(16) Theil, E. C., Behera, R. K., and Tosha, T. (2013) Ferritins for chemistry and for life. *Coord. Chem. Rev. 257*, 579−586.

(17) Pereira, A. S., Small, W., Krebs, C., Tavares, P., Edmondson, D. E., Theil, E. C., and Huynh, B. H. (1998) Direct spectroscopic and kinetic evidence for the involvement of a peroxodiferric intermediate during the ferroxidase reaction in fast ferritin mineralization. *Biochemistry 37*, 9871−9876.

(18) Moënne-Loccoz, P., Krebs, C., Herlihy, K., Edmondson, D. E., Theil, E. C., Huynh, B. H., and Loehr, T. M. (1999) The ferroxidase reaction of ferritin reveals a diferric μ-1,2 bridging peroxide intermediate in common with other O_2-activating non-heme diiron proteins. *Biochemistry 38*, 5290−5295.

(19) Takagi, H., Shi, D., Ha, Y., Allewell, N. M., and Theil, E. C. (1998) Localized unfolding at the junction of three ferritin subunits. A mechanism for iron release? *J. Biol. Chem. 273*, 18685−18688.

(20) Ha, Y., Shi, D., Small, G. W., Theil, E. C., and Allewell, N. M. (1999) Crystal structure of bullfrog M ferritin at 2.8 Å resolution: analysis of subunit interactions and the binuclear metal center. *J. Biol. Inorg. Chem. 4*, 243−256.

(21) Hwang, J., Krebs, C., Huynh, B. H., Edmondson, D. E., Theil, E. C., and Penner-Hahn, J. E. (2000) A short Fe-Fe distance in peroxodiferric ferritin: control of Fe substrate versus cofactor decay? *Science 287*, 122−125.

(22) Liu, X., and Theil, E. C. (2004) Ferritin reactions: Direct identification of the site for the diferric peroxide reaction intermediate. *Proc. Natl. Acad. Sci. U.S.A. 101*, 8557−8562.

(23) Theil, E. C. The ferritin protein nanocage and biomineral, from single Fe atoms to FeO nanoparticles: Starting with EXAFS.*AIP Conf. Proc.* 2007, *882*, 15−18.

(24) Schwartz, J. K., Liu, X. S., Tosha, T., Theil, E. C., and Solomon, E. I. (2008) Spectroscopic definition of the ferroxidase site in M ferritin: comparison of binuclear substrate vs cofactor active sites. *J. Am. Chem. Soc. 130*, 9441−9450.

(25) Tosha, T., Hasan, M. R., and Theil, E. C. (2008) The ferritin Fe2 site at the diiron catalytic center controls the reaction with O_2 in the rapid mineralization pathway. *Proc. Natl. Acad. Sci. U.S.A. 105*, 18182−18187.

(26) Turano, P., Lalli, D., Felli, I. C., Theil, E. C., and Bertini, I. (2010) NMR reveals pathway for ferric mineral precursors to the central cavity of ferritin. *Proc. Natl. Acad. Sci. U.S.A. 107*, 545−550.

(27) Tosha, T., Ng, H.-L., Bhattasali, O., Alber, T., and Theil, E. C. (2010) Moving metal ions through ferritin-protein nanocages from three-fold pores to catalytic sites. *J. Am. Chem. Soc. 132*, 14562−14569.

(28) Tosha, T., Behera, R. K., Ng, H.-L., Bhattasali, O., Alber, T., and Theil, E. C. (2012) Ferritin protein nanocage ion channels: gating by N-terminal extensions. *J. Biol. Chem. 287*, 13016−13025.
(29) Tosha, T., Behera, R. K., and Theil, E. C. (2012) Ferritin ion channel disorder inhibits Fe(II)/O_2 reactivity at distant sites. *Inorg. Chem. 51*, 11406−11411.
(30) Bertini, I., Lalli, D., Mangani, S., Pozzi, C., Rosa, C., Theil, E. C., and Turano, P. (2012) Structural insights into the ferroxidase site of ferritins from higher eukaryotes. *J. Am. Chem. Soc. 134*, 6169−6176.
(31) Crow, A., Lawson, T. L., Lewin, A., Moore, G. R., and Le Brun, N. E. (2009) Structural basis for iron mineralization by bacterioferritin. *J. Am. Chem. Soc. 131*, 6808−6813.
(32) Solomon, E. I., Brunold, T. C., Davis, M. I., Kemsley, J. N., Lee, S.-K., Lehnert, N., Neese, F., Skulan, A. J., Yang, Y.-S., and Zhou, J. (2000) Geometric and electronic structure/function correlations in non-heme iron enzymes. *Chem. Rev. 100*, 235−350.
(33) Schwartz, J. K. (2008) *Spectroscopic and Theoretical Elucidation of Structural Contribution to Reactivity in Binuclear Non-Heme Iron Enzymes: Substrate versus Cofactor Sites* (Solomon, E. I., Ed.) Stanford University.
(34) Reem, R. C., and Solomon, E. I. (1987) Spectroscopic studies of the binuclear ferrous active site of deoxyhemerythrin: coordination number and probable bridging ligands for the native and ligand-bound forms. *J. Am. Chem. Soc. 109*, 1216−1226.
(35) Hagen, K. S., and Lachicotte, R. (1992) Diiron (II) μ-aqua bis (μ-carboxylato) models of reduced dinuclear non-heme iron sites in proteins. *J. Am. Chem. Soc. 114*, 8741−8742.
(36) Brunold, T. C., and Solomon, E. I. (1999) Reversible dioxygen binding to hemerythrin. 1. Electronic structures of deoxy-and oxyhemerythrin. *J. Am. Chem. Soc. 121*, 8277−8287.
(37) Wei, P.-P., Skulan, A. J., Wade, H., DeGrado, W. F., and Solomon, E. I. (2005) Spectroscopic and computational studies of the de novo designed protein DF2t: Correlation to the biferrous active site of ribonucleotide reductase and factors that affect O_2 reactivity. *J. Am. Chem. Soc. 127*, 16098−16106.
(38) Frisch, M. J., et al. *Gaussian 09*, revision D.01; Gaussian, Inc., Wallingford CT, 2009.
(39) Voegtli, W. C., Sommerhalter, M., Saleh, L., Baldwin, J., Bollinger, J. M., and Rosenzweig, A. C. (2003) Variable coordination geometries at the diiron(II) active site of ribonucleotide reductase R2. *J. Am. Chem. Soc. 125*, 15822−15830.
(40) Theil, E. C. (2011) Ferritin protein nanocages use ion channels, catalytic sites, and nucleation channels to manage iron/oxygen chemistry. *Curr. Opin. Chem. Biol. 15*, 304−311.